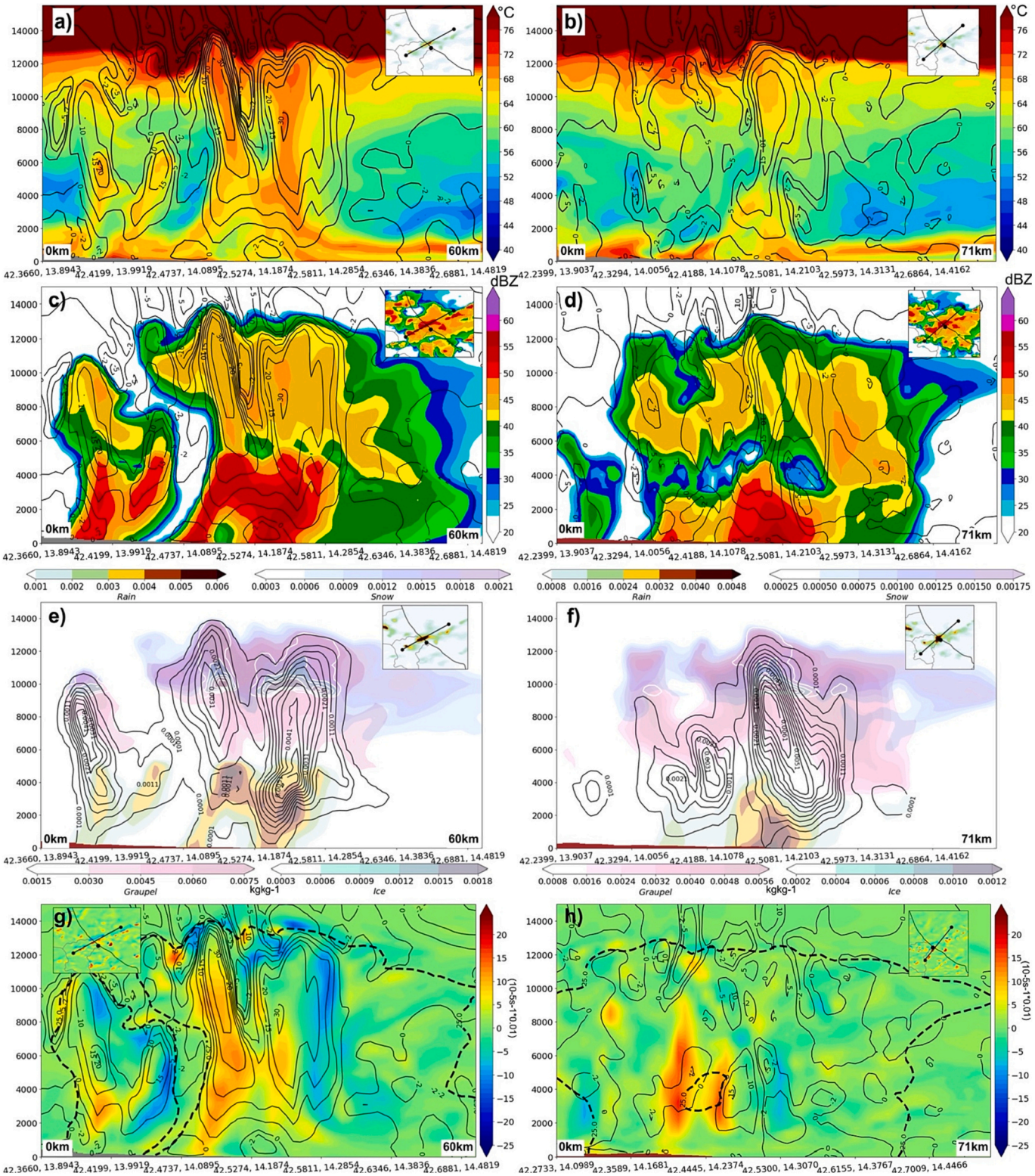

Fig. 8. As in Fig. 7, except for the cross sections along the track highlighted in the sub-panels; panels a-c-e-g refer to the time 10:20 UTC, panels b-d-f-h refer to 10:30 UTC.

up to 14 km. East of the cell a marked Bounded Weak Echo Region (BWER) (Heymsfield and Musil 1982) with reflectivity ranging from 40 to 45 to 25-30dBZ is found (Figs. 7c-d, blue areas), whereas Weak Echo Regions (WER) are also found near the surface. This seems to be in a fair agreement with the radar cross section (Fig. 3c) both in terms of BWER and its vertical extention suggesting a good ability of the model in reproducing the observed vertical wind strength. Note that Fig. 3d shows a vertical structure of a companion cell that our simulations were not able to correctly reproduce. The WER are associated with the hail maximum (Fig. 7e,f, solid contours), and are typical of supercells. Rain is found (Figs. 7 e,f) below the updraft (further back) up to 6 km, whereas hail is found from the ground to the top of the supercell (16 km). The

maximum hail values are correctly produced in the BWER, indicating a strong rotation of the updraft in this area, and a vertical hook structure, in the direction of storm propagation, as Figs. 9a-b confirm. Above 6 km, widespread graupel is found throughout the structure, whereas a blanket of snow is found from 8 km to the top of the cell (Fig. 7e,f, light violet and blue respectively) in agreement with the formation of new hydrometeors during the vertical development of the cell. Within the most intense area of the cell up to 10–16 km, a large concentration of ice with a maximum at 11 km is found (Figs. 7e,f, gray and white contour). The absolute vorticity assumes high positive values (+15 s^{-1}) along the boundary of the updraft and negative values along the downdraft (−15 s^{-1}, Figs. 7g, h and Figs. 9a,b). The west-east cross section along the line joining the two cells shows how they interact with each other producing an intense downdraft in the areas where the largest precipitation of rain and hail reach the ground. The RFD over the sea produces an additional trigger to the cell arriving from the coast, intensifying it (Figs. 9a-c).

Between 10:20 and 10:30UTC (Figs. 5m,n) the two storm cells merge into a single one. The merging, during this transition stage, of the two cells is identified by the structure and distribution of reflectivity and rainfall that clearly show a single storm system (Figs. 5d,f). In this phase, despite the unified precipitation, hydrometeor, and reflectivity (Fig. 8c, d and e, f), the thermodynamic and dynamical structure still show two separate updrafts, interacting with each other (Fig. 8a). The updraft of the main cell is more intense, exceeds 35 ms^{-1} with the maximum between 8 and 12 km, and it continues to sustain the overshooting top (height exceeding 14 km), as shown in Fig. 8a,b and Fig_suppl_2c,d. The maxima of Θ_e are found in the core of the updraft between 6 and 12 km (Fig. 8a). This suggests that the cell continues to be fed through the release of latent heat of condensation, albeit to a lesser extent than in the phase of maximum intensity. As shown in Rotunno et al. (2017), the low level high horizontal vorticity that characterizes the area on the sea and near the coast, is transformed into vorticity helicity (cork-screw like motion) inside the most intense cell.

Entering from the sea, there is a second cell characterized by a weaker vertical velocity (20-25 ms^{-1}) but associated with high Θ_e values in the center of the updraft. The "Forward Flank Downdraft" is between the two cells characterized by an intense downdraft reaching −5 ms^{-1} at 5–12 km (Fig. 8a). The vertical cut of the radar at Il Monte clearly shows both the second cell and the FFD (Fig. 3c). At upper levels, on the rear of the updraft of the first cell, the "Rear Flank Downdraft "is found a very intense downdraft (> −15 ms^{-1}) with a maximum between 10 and 12 km. The RFD is characterized by large vertical descending motion, vertically extended through a deep layer and localized in space (Davies-Jones, 1984, Davies-Jones, 2023, Markowski et al., 2002, Trapp and Davies-Jones, 1997, Trapp et al., 2005). At 10:20 UTC, the reflectivity highlights a very complex structure typical of the supercells, with an extended BWER in the front, close to the ground (Fig. 8c) and another one at 10:30 UTC (Fig. 8d, white area) at 4 km as found in the vertical cut of the radar (Fig. 3c) at 10:40 UTC. From 10:30 UTC, the storm starts to decay: the weakening of the vertical speeds is observed with maximum values of 15–20 ms^{-1} between 6 and 11 km height in front of the supercell and around −20 ms^{-1} in the rear at heights 10–15 km (and Fig_suppl_2d), as well as a decrease in Θ_e values in the core of the cell. The structure has merged into a single cell, with a single updraft in the center and a downdraft below the storm cell (Figs. 8 b,d). The hydrometeors show a wider spatial distribution at the ground and at relatively lower altitudes, supporting the interpretation of the storm entering its decay phase. In particular, the cell produces a smaller amount of solid hydrometeors, and a sharp increase in the amount of liquid precipitation at the ground reaching 40 mm in 10 min.

In what follows the analysis of the 3D structure of the supercell at 10:10UTC is performed by using the software Vapor (Fig. 9) (www.vapor.ucar.edu, Li et al., 2019) with the aim of qualitatively analyzing it. The interaction of the air masses flow, between the two cells is clearly shown by the 3D structure (Fig. 9a,b). The supercell, oriented perpendicular to the coast, shows an interaction between tree air masses that wrapping each other, in anti-clockwise motion a typical flow dynamics of supercells, as shown in Miglietta et al. (2016).

5. Hail and hail size prediction model

As discussed in the previous section, the supercell that developed on July 9–10, 2019 was a very severe event especially in terms of hail quantity and dimension. The hailstones reaching the ground had a diameter of approximately 10–14 cm characterized by a smooth and wet surface.

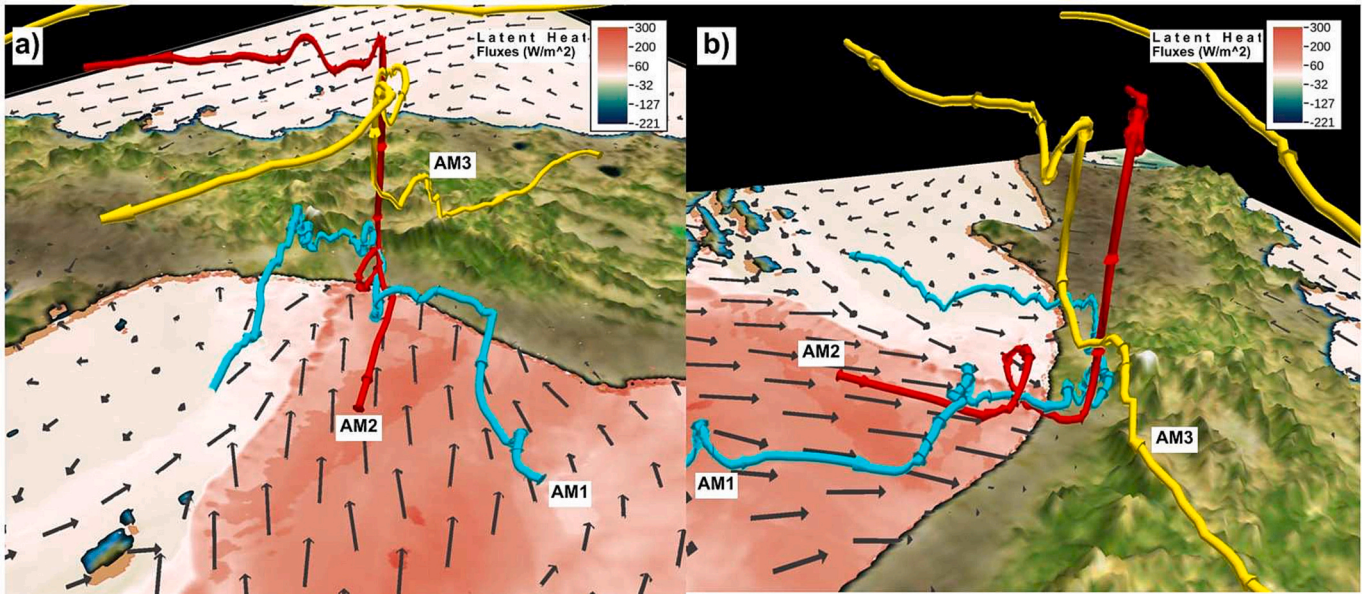

Figs. 9. Panels a-b show the vertical structure of the supercell (using Vapor www.vapor.ucar.edu, Li et al., 2019) during the developing stage (10:20UTC);. The color represents air maxes defined in Ricchi et al., 2023. AM1 is a relative dry and cold Bora air that came from Dinaric Alps; AM2 is a warm, wet and unstable air mass that advect from south Adriatic Sea, over storm developing area. AM3 is an air mass that came from northwest, blocked by Apennines, as shown in Fig. 19, in Ricchi et al., 2023. In panel a,b is showed the trajectory of air masses that wrapping in a supercell rotating system. Vectors represent wind direction al 10 m and shaded color over sea represent latent heat fluxes at air-sea interface (positive value represent fluxes from sea to atmosphere).

Unfortunately, the lack of this kind of observation in the area of the event did not allow us to perform the tuning of the algorithm. Note that even though the default configuration (continental CCN) was used, HAILCAST fairly estimated the size and the position of the hail (a diameter of 7–8 cm, Figs. 10a - c), in the most intense phase of the event (10:00–10:30UTC). The size of the hail at the ground was approximately 10 cm in diameter, hence HAILCAST slightly underestimates them, but this was expected because the key role played by the initial seeds in producing the hail size. In particular, Adams-Selin and Ziegler (2016) pointed out that the HAILCAST tuning is based on inland observation, whereas this storm developed along the coast, with a strong component coming from the sea. Therefore, maritime aerosols and marine sprays are expected to be part of the air mass, impacting not only the energy fluxes at the air-sea interface (Rizza et al., 2018), but also the type of particles suspended in the cloud. As demonstrated by Ilotoviz et al., 2018, increasing the concentration of aerosols in the cloud increases the content of supercooled water and this favors the growth of wet hail. This event was characterized by air coming from the open sea as well as from inland, hence it was not characterized by a well-defined air mass seeding the cell. This is why in the present study it was decided not to change the characteristics of the seeds; this will be done in a later study dedicated to the sensitivity to this parameter.

According to the United States Meteorological Service in order to generate and maintain in suspension hail of size >10 cm, slightly rough and wet, the updraft must be close to or larger than 45-50 ms^{-1}. The results of this study show that the updraft speeds simulated by the model are consistent with the theory. This is an indirect way of assessing whether the model simulated vertical velocities are realistic. Moreover, there is also a large amount of hail and ice in the updraft, even at altitudes where the maximum vertical speed is observed (between 8000 and 12,500 m).

In the development phase of the supercell, the accumulated hail at the ground (Fig. 10a, contour line) reaches only 1 mm. This suggests that the giant hailstones are still held in suspension at high altitude by the large vertical velocity, and these large values are in perfect agreement with the theory, as it takes approximately 50 ms^{-1} to maintain hailstones close to 10 cm in size at high altitude. In the mature phase of the supercell, the hail content in the cloud increases (Figs. 8e,f), exceeding 0.0041 $kgkg^{-1}$, whereas the size of the hailstones decreases slightly (Figs. 10a-c respectively) with respect to the developing phase. The hail begins to fall accumulating approximately 5–7 mm at the ground with a maximum at 4000 m (Figs. 8e,f). These two maxima correspond to the BWER at the ground and the one between the downdraft and the updraft, in the lower levels of the atmosphere (Fig. 8c-d, blue areas respectively). The hail at the lower level and the hail at the ground are located in the front of the updraft and in the direction of propagation of the cell which is still tilted forward.

6. Conclusions

Many physical mechanisms influence the predictability and the ability of numerical models to reproduce extreme weather phenomena like supercells. Still these factors are not completely understood or correctly represented in the numerical models (Manzato et al., 2020; Tiesi et al., 2022). Therefore, the mechanisms underlying the development and intensification of the supercell formed along the coast of the Abruzzo region, on 10 July 2019 (Montopoli et al., 2021; Tiesi et al., 2022) is investigated. The supercell moved along the coast and produced intense winds, precipitation (100-130 mm/h) and large hail (10-12 cm in diameter). A storm cell developing and moving along the coast is not unusual in this area but it is extremely rare to observe such significant extreme phenomena as a supercell. In order to investigate the 3D structure of the supercell from the triggering to the decay phase, the WRF numerical model is used in the best configuration as defined by Ricchi et al. (2023) with high resolution (grid spacing of 1 km) and a correction of both the topography and the SST. In the companion paper, Ricchi et al. (2023) assessed the role of both the height of the mountain and the SST. A correction of the altitude of the mountain peaks, in particular Sibillini and Gran Sasso, had to be placed in the model topography to obtain the correct location, intensity, dynamics and morphology of the storm cell. Moreover, the use of the SST at 1 km resolution (GOS HR 1 km, Buongiorno Nardelli et al., 2013) is the only one that allowed reproducing the storm cell at the same times as observed, with a cell elongated perpendicular to the coast and moving from north to south.

The main question investigated in this work is the investigation of a supercell using the WRF model. In particular to investigate if the WRF model at high resolution is able to reproduce the dynamics and thermodynamics of a supercell characterized by strong hail production. The observations and the model results confirm the supercellular nature of the storm (as already shown by Montopoli et al., 2021 and Tiesi et al., 2022) and that the WRF numerical model can reproduce not only the patterns and physical signatures, but also the 3D observed structures, typical of a supercell. The vertical structure of the supercell shows two separate updrafts, a principal one on the coast and the secondary one offshore. The main one has a tilted axis, that is a necessary condition for producing rain without the supercell updraft destroying itself, and to maintain and sustain the formation of giant hail at upper layers with a strong updraft. In particular, the model can reproduce the hail and ice at very high altitudes (>8 km) as shown in Montopoli et al. (2021), as well

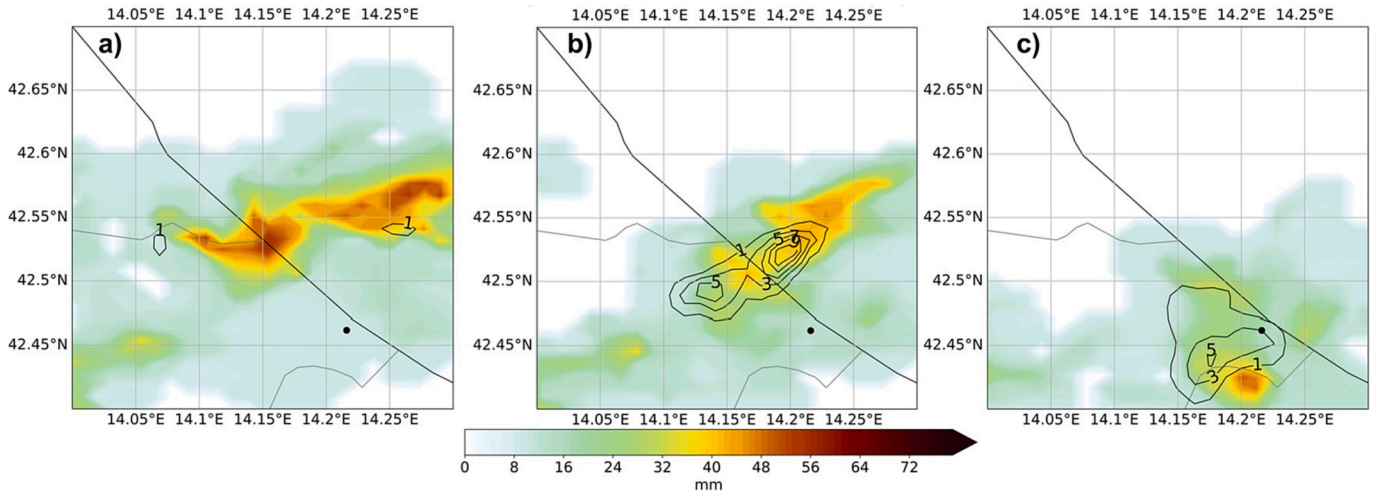

Fig. 10. The accumulated hail on the ground (contour line), at the reference instants 10:10 UTC, 10: 20 UTC and 10:30 UTC, and the size of the hail (shaded) in cm.

as the intense updrafts with vertical velocity up to 40-50 ms^{-1}, which are necessary to maintain smooth hail (low drag coefficient) of a size >8-10 cm in suspension (as suggested by National Weather Service and NOAA guideline, and in numerous papers such as Atlas, 1966). Moreover, the three-dimensional analysis, using VAPOR, allowed the identification of two different structures of updraft. In the development stage, during its maximum intensity, the updraft shows a very large vertical velocity, anti-clockwise rotation and a tubular horizontal structure, which merges into the updraft with negative vorticity. In the transition phase, from development to maturity, the tubular structure divides into two cones, one with positive vorticity and one with negative vorticity. The main structure of the updraft shows counterclockwise rotation, and absolute positive vorticity, the lateral one shows negative vorticity, in continuity with the rotation propagating from the ground and insinuating itself into this updraft, as shown in Klemp (1987). There is a complex updraft structure: between 1500 and 6000 m, there are net vertical velocities of approximately 20 ms^{-1}; above 6000 m the updraft stops rotating and it reaches vertical speeds of 40-50 ms^{-1} up to 8000-9000 m. Furthermore, a counterclockwise rotation is found for the whole system, which suggests that the system was assuming mesocyclone characteristics. This event produced large hail (>5 cm), represented with an error of 20–30% by the HAILCAST module. This is a fairly good result if we consider that HAILCAST must be calibrated for this area. This was not possible because of the lack of observations and/or field campaigns in this area where extreme hailstorms are very rare. Eventually, the default configuration provides a useful means for forecasters to understand in advance whether hail can exceed certain thresholds, with an acceptable error. Further analyses of HAILCAST will be carried out, considering other events with hail of various sizes, in order to evaluate the error and its trend as the hail builds up on this basin.

In summary, the most important results of this study are the following:

- The need for high horizontal and vertical resolution to correctly reproduce the supercell was established; a high frequency sampling of the model output (10 min) was necessary to capture the supercell and to investigate and analyze it.
- There is a fundamental role played by the parametrization of the microphysics, which must implement a sufficient number of hydrometeors, among them hail (see Manzato et al., 2020).
- This study is one of the few to represent a real coastal supercell using a numerical model over this area, at this spatio-temporal resolution, investigating in-depth the supercell structure using a hundred vertical levels, and a complete hydrometeors class that characterize a summer supercell.
- This work lays the foundations for the study of other similar events over the European area, which has cells not often identified as supercells due to the lack of observations or the use of low-resolution, space-time models.
- Comparison with radar data suggests a general agreement with the simulations in terms of the timing and structure of the event. In terms of dynamics, the horizontal mesocyclone signature is well reproduced as well as the signatures of WER and BWER, proxies of vertical updraft structure
- The HAILCAST module adequately reproduces the size of the hail, even though it needs to be calibrated, in particular according to the type of seeds and condensation nuclei present in the studied area, i.e. of land or marine origin. Furthermore, the HAILCAST model, properly configured, can be very useful in NWP applications, in particular in a climatic context of increasing extreme events, both for scientific and socio-economic applications. Hence, the forecast complexity is intrinsic in operational modeling and attempts to use machine-learning for the daily choice of numerical schemes (Schultz et al., 2021) made only recently, may be a possibility for improving the weather forecast.
- The physical and morphological representation of the supercell investigated in this paper, was made possible by particularly high-performance and accurate numerical simulation.

Finally, in this work, high quality representation of the storm, starting from a large set of simulations tested, characterized by different physical and numerical configurations (not shown) is produced.

Therefore, few important outcomes for improving the operational forecasting predictability of supercell events, that can be particularly low, in coastal transitional areas, where the influence of the sea and orography can be significant (Davolio et al., 2009; Cassola et al., 2016; Ricchi et al., 2021) are the following:

1) The impact of the Millbrandt double-moment microphysics (Milbrandt and Yau, 2005) plays a crucial role in the accurate simulation of the supercell structure, most likely because the simulation can reproduce all the hydrometeors that play a role in the thermodynamics of deep convection.
2) To properly discriminate, not only the dynamics of the PBL (Planetary Boundary Layer) but also that of the mid and upper atmosphere, it is crucial to use many vertical levels, in this work we used 100 vertical levels (not shown).
3) The impact of the integration timestep, a small timestep (close to 1*resolution) was necessary to improve the simulation in term of rainfall accumulation and localization (not shown).

All these features of the present simulation, combined with the high horizontal resolution of the numerical grid, are often prohibitive for operational forecasting.

CRediT authorship contribution statement

Antonio Ricchi: Conceptualization, Investigation, Methodology, Data curation, Formal analysis, Writing – original draft, Writing – review & editing. **Richard Rotunno:** Visualization, Investigation, Supervision. **Mario Marcello Miglietta:** Investigation, Writing – review & editing. **Errico Picciotti:** Data curation. **Mario Montopoli:** Data curation, Writing – original draft, Writing – review & editing. **F.S. Marzano:** Methodology, Data curation. **Luca Baldini:** Writing – review & editing. **Gianfranco Vulpiani:** Data curation. **Alessandro Tiesi:** Writing – original draft, Data curation. **Rossella Ferretti:** Funding acquisition, Supervision, Writing – original draft, Writing – review & editing.

Declaration of Competing Interest

The authors declare that the research was conducted in the absence of any commercial or financial relationships that could be construed as a potential conflict of interest.

Data availability

Data will be made available on request.

Acknowledgments

The research described in this paper has been developed in the framework of the research project National Centre for HPC, Big Data and Quantum Computing - PNRR Project, funded by the European Union - Next Generation EU and by the Special Project ASIM-CPL founded by ECMWF. Dr. Antonio Ricchi (University of L'Aquila/CETEMPS) is funded by PON - DM1062 Project and from PON Ricerca e Innovazione 2014–2020 “AIM”—Attraction and international mobility program. EU Social Fund and Regional Development Fund; Ministero dell'Istruzione e della Ricerca, grant number AIM1858058.

Appendix A. Supplementary data

Supplementary data to this article can be found online at https://doi.org/10.1016/j.atmosres.2023.107079.

References

Adams-Selin, R.D., Ziegler, C.L., 2016. Forecasting hail using a one-dimensional hail growth model within WRF. Mon. Weather Rev. 144 (12), 4919–4939. https://doi.org/10.1175/MWR-D-16-0027.1.

Adams-Selin, R.D., Clark, A.J., Melick, C.J., Dembek, S.R., Jirak, I.L., Ziegler, C.L., 2019. Evolution of WRF-HAILCAST during the 2014–16 NOAA/hazardous Weather Testbed Spring forecasting experiments. Weather Forecast. 34 (1), 61–79. https://doi.org/10.1175/WAF-D-18-0024.1.

Adams-Selin, R.D., Ziegler, C.L., 2016. Forecasting Hail Using a One-Dimensional Hail Growth Model within WRF. Monthly Weather Review 144 (12), 4919–4939. https://doi.org/10.1175/MWR-D-16-0027.1.

Aminou, D.M.A., Ottenbacher, A., Hanson, C.G., Pili, P., Muller, J., Blancke, B., Jacquet, B., Bianchi, S., Coste, P., Pasternak, F., Faure, F., 2003. In: Barnes, W.L. (Ed.), Meteosat Second Generation: The MSG-1 Imaging Radiometer Performance Results at the End of the Commissioning Phase, p. 599. https://doi.org/10.1117/12.505866.

Atlas, & David., 1966. The Balance Level in Convective Storms. JAtS 23 (6), 635–651. https://doi.org/10.1175/1520-0469(1966)023.

Baldi, M., Ciardini, V., Dalu, J.D., de Filippis, T., Maracchi, G., Dalu, G., 2014. Hail occurrence in Italy: Towards a national database and climatology. Atmos. Res. 138, 268–277. https://doi.org/10.1016/j.atmosres.2013.11.012.

Barbieri, S., Di Fabio, S., Lidori, R., Rossi, F.L., Marzano, F.S., Picciotti, E., 2022. Mosaicking weather radar retrievals from an operational heterogeneous network at C and X band for precipitation monitoring in Italian Central Apennines. Remote Sens. 14, 248. https://doi.org/10.3390/rs14020248.

Brimelow, J.C., Reuter, G.W., 2009. Explicit forecasts of hail occurrence and expected hail size using the GEM-HAILCAST system with a rainfall filter. Weather Forecast. 24 (4), 935–945. https://doi.org/10.1175/2009WAF2222138.1.

Buongiorno Nardelli, B., Tronconi, C., Pisano, A., Santoleri, R., 2013. High and Ultra-High resolution processing of satellite Sea Surface Temperature data over southern European Seas in the framework of MyOcean project. Remote Sens. Environ. 129, 1–16. https://doi.org/10.1016/j.rse.2012.10.012.

Capozzi, V., Picciotti, E., Mazzarella, V., Marzano, F.S., Budillon, G., 2017. Fuzzy-logic detection and probability of hail exploiting short-range X-band weather radar. Atmospheric Research 201, 17–33. https://doi.org/10.1016/j.atmosres.2017.10.006.

Cassola, F., Ferrari, F., Mazzino, A., Miglietta, M.M., 2016. The role of the sea on the flash floods events over Liguria (northwestern Italy). Geophys. Res. Lett. 43 (7), 3534–3542. https://doi.org/10.1002/2016GL068265.

Davies-Jones, R., 1984. Streamwise vorticity: the origin of updraft rotation in supercell storms. J. Atmos. Sci. 41 (20), 2991–3006. https://doi.org/10.1175/1520-0469(1984)041<2991:SVTOOU>2.0.CO;2.

Davies-Jones, R., 2023. 2.2 Tornadogenesis in Supercell Storms-What we Know and What we Don't Know.

Davolio, S., et al., 2009. High resolution simulations of a flash flood near Venice. Nat. Hazards Earth Syst. Sci. 9 (5), 1671–1678. https://doi.org/10.5194/nhess-9-1671-2009.

Dotzek, N., Groenemeijer, P., Feuerstein, B., Holzer, A.M., 2009. Overview of ESSL's severe convective storms research using the European Severe Weather Database ESWD. Atmos. Res. 93 (1–3), 575–586. https://doi.org/10.1016/j.atmosres.2008.10.020.

Dudhia, J., 1989. Numerical study of convection observed during the winter monsoon experiment using a mesoscale two-dimensional model. J. Atmos. Sci. 46 (20), 3077–3107. https://doi.org/10.1175/1520-0469(1989)046<3077:NSOCOD>2.0.CO;2.

Fluck, E., Kunz, M., Geissbuehler, P., Ritz, S.P., 2021. Radar-based assessment of hail frequency in Europe. Nat. Hazards Earth Syst. Sci. 21 (2), 683–701. https://doi.org/10.5194/nhess-21-683-2021.

Galanaki, E., Lagouvardos, K., Kotroni, V., Flaounas, E., Argiriou, A., 2018. Thunderstorm climatology in the Mediterranean using cloud-to-ground lightning observations. Atmos. Res. 207, 136–144. https://doi.org/10.1016/j.atmosres.2018.03.004.

Ilotoviz, E., Khain, A., Ryzhkov, A., Snyder, J.C., 2018. Relationship between aerosols, Hail Microphysics, and ZDR Columns. J. Atmos. Sci. 75 (6), 1755–1781. https://doi.org/10.1175/JAS-D-17-0127.1.

Iocca, F., Lazzeri, M., Pellegrini, M., 2023. Open-source data processing chain for marche region X-band weather radar. J. Electron. Electr. Eng. 2, 44–57.

Janjić, Z.I., 1994. The step-mountain eta coordinate model: further developments of the convection, viscous sublayer, and turbulence closure schemes. Mon. Weather Rev. 122 (5), 927–945. https://doi.org/10.1175/1520-0493(1994)122<0927:TSMECM>2.0.CO;2.

Jurković, P.M., Mahović, N.S., Počakal, D., 2015. Lightning, overshooting top and hail characteristics for strong convective storms in Central Europe. Atmosph. Res. 161–162, 153–168. https://doi.org/10.1016/J.ATMOSRES.2015.03.020.

Kahraman, A., Kendon, E.J., Chan, S.C., Fowler, H.J., 2021. Quasi-Stationary Intense Rainstorms Spread Across Europe Under Climate Change. Geophys. Res. Lett. 48 (13), e2020GL092361 https://doi.org/10.1029/2020GL092361.

Klemp, J.B., 1987. Dynamics of Tornadic Thunderstorms. Annu. Rev. Fluid Mech. 19 (1), 369–402. https://doi.org/10.1146/annurev.fl.19.010187.002101.

Kunz, M., Kugel, P.I.S., 2015. Detection of hail signatures from single-polarization C-band radar reflectivity. Atmosph. Res. 153, 565–577. https://doi.org/10.1016/J.ATMOSRES.2014.09.010.

Laviola, S., Monte, G., Levizzani, V., Ferraro, R.R., Beauchamp, J.A., 2020. New method for hail detection from the GPM constellation: a prospect for a global hailstorm climatology. Remote Sens. 12, 3553. https://doi.org/10.3390/rs12213553.

Li, S., Jaroszynski, S., Pearse, S., Orf, L., Clyne, J., 2019. VAPOR: a visualization package tailored to analyze simulation data in earth system science. Atmosphere. 10 (9), 488. https://doi.org/10.3390/atmos10090488.

Manzato, A., Riva, V., Tiesi, A., Marcello Miglietta, M., 2020. Observational analysis and simulations of a severe hailstorm in northeastern Italy. Quarterly Journal of the Royal Meteorological Society 146 (732), 3587–3611. https://doi.org/10.1002/QJ.3886.

Markowski, P.M., Straka, J.M., Rasmussen, E.N., 2002. Direct surface thermodynamic observations within the rear-flank downdrafts of nontornadic and tornadic supercells. Mon. Weather Rev. 130 (7), 1692–1721. https://doi.org/10.1175/1520-0493(2002)130<1692:DSTOWT>2.0.CO;2.

Marra, A.C., Porcù, F., Baldini, L., Petracca, M., Casella, D., Dietrich, S., Mugnai, A., Sanò, P., Vulpiani, G., Panegrossi, G., 2017. Observational analysis of an exceptionally intense hailstorm over the Mediterranean area: Role of the GPM Core Observatory. Atmos. Res. 192, 72–90. https://doi.org/10.1016/j.atmosres.2017.03.019.

Meroni, A.N., Parodi, A., Pasquero, C., 2018. Role of SST patterns on surface wind modulation of a heavy midlatitude precipitation event. J. Geophys. Res. Atmos. 123 (17), 9081–9096. https://doi.org/10.1029/2018JD028276.

Miglietta, M.M., Davolio, S., 2022. Dynamical forcings in heavy precipitation events over Italy: Lessons from the HyMeX SOP1 campaign. Hydrol. Earth Syst. Sci. 26 (3), 627–646. https://doi.org/10.5194/HESS-26-627-2022.

Miglietta, M.M., Manzato, A., Rotunno, R., 2016. Characteristics and predictability of a supercell during HyMeX SOP1. Q. J. R. Meteorol. Soc. 142 (700), 2839–2853. https://doi.org/10.1002/qj.2872.

Miglietta, M.M., Mazon, J., Motola, V., Pasini, A., 2017. Effect of a positive Sea Surface Temperature anomaly on a Mediterranean tornadic supercell. Sci. Rep. 7 (1), 12828. https://doi.org/10.1038/s41598-017-13170-0.

Milbrandt, J.A., Yau, M.K., 2005. A multimoment bulk microphysics parameterization. Part I: analysis of the role of the spectral shape parameter. J. Atmos. Sci. 62 (9), 3051–3064. https://doi.org/10.1175/JAS3534.1.

Mlawer, E.J., Taubman, S.J., Brown, P.D., Iacono, M.J., Clough, S.A., 1997. Radiative transfer for inhomogeneous atmospheres: RRTM, a validated correlated-k model for the longwave. J. Geophys. Res. Atmos. 102 (D14), 16663–16682. https://doi.org/10.1029/97JD00237.

Mohr, S., Kunz, M., Geyer, B., 2015. Hail potential in Europe based on a regional climate model hindcast. Geophys. Res. Lett. 42 (24), 10,904–10,912. https://doi.org/10.1002/2015GL067118.

Montopoli, M., Picciotti, E., Baldini, L., di Fabio, S., Marzano, F.S., Vulpiani, G., 2021. Gazing inside a giant-hail-bearing Mediterranean supercell by dual-polarization Doppler weather radar. Atmos. Res. 264, 105852 https://doi.org/10.1016/j.atmosres.2021.105852.

Morcrette, J.-J., Boucher, O., Jones, L., Salmond, D., Bechtold, P., Beljaars, A., Benedetti, A., Bonet, A., Kaiser, J.W., Razinger, M., Schulz, M., Serrar, S., Simmons, A.J., Sofiev, M., Suttie, M., Tompkins, A.M., Untch, A., 2009. Aerosol analysis and forecast in the European Centre for Medium-Range Weather Forecasts Integrated Forecast System: Forward modeling. J. Geophys. Res. 114 (D6), D06206. https://doi.org/10.1029/2008JD011235.

Nelson, S.P., 1983. The influence of storm flow structure on hail growth. J. Atmos. Sci. 40 (8), 1965–1983. https://doi.org/10.1175/1520-0469(1983)040<1965:TIOSFS>2.0.CO;2.

Púčik, T., Castellano, C., Groenemeijer, P., Kühne, T., Rädler, A.T., Antonescu, B., Faust, E., 2019. Large hail incidence and its economic and societal impacts across Europe. Mon. Weather Rev. 147 (11), 3901–3916. https://doi.org/10.1175/MWR-D-19-0204.1.

Punge, H.J., Kunz, M., 2016. Hail observations and hailstorm characteristics in Europe: a review. Atmos. Res. 176–177, 159–184. https://doi.org/10.1016/j.atmosres.2016.02.012.

Qiao, X., Wang, S., Min, J., 2018. The impact of a stochastically perturbing microphysics scheme on an idealized supercell storm. Mon. Weather Rev. 146 (1), 95–118. https://doi.org/10.1175/MWR-D-17-0064.1.

Ricchi, A., Bonaldo, D., Cioni, G., Carniel, S., Miglietta, M.M., 2021. Simulation of a flash-flood event over the Adriatic Sea with a high-resolution atmosphere–ocean–wave coupled system. Sci. Rep. 11 (1), 9388. https://doi.org/10.1038/s41598-021-88476-1.

Ricchi, Antonio, Sangelantoni, Lorenzo, Redaelli, Gianluca, Mazzarella, Vincenzo, Montopoli, Mario, Miglietta, Mario Marcello, Tiesi, Alessandro, Mazzà, Simone, Rotunno, Richard, Ferretti, Rossella, 2023. Impact of the Sst and Topography on the Development of a Large-hail Storm Event, on the Adriatic Sea. Available at SSRN: https://ssrn.com/abstract=4482004 https://doi.org/10.2139/ssrn.4482004.

Rizza, U., Canepa, E., Ricchi, A., Bonaldo, D., Carniel, S., Morichetti, M., Passerini, G., Santiloni, L., Scremin Puhales, F., Miglietta, M., 2018. Influence of wave state and sea spray on the roughness length: feedback on medicanes. Atmosphere 9 (8), 301. https://doi.org/10.3390/atmos9080301.

Rotunno, R., 1993. Supercell thunderstorm modeling and theory, pp. 57–73. https://doi.org/10.1029/GM079p0057.

Rotunno, R., Markowski, P.M., Bryan, G.H., 2017. “Near ground” vertical vorticity in supercell thunderstorm models. J. Atmos. Sci. 74 (6), 1757–1766. https://doi.org/10.1175/JAS-D-16-0288.1.

Schultz, M.G., Betancourt, C., Gong, B., Kleinert, F., Langguth, M., Leufen, L.H., Mozaffari, A., Stadtler, S., 2021. Can deep learning beat numerical weather prediction? Philosophical Transactions of the Royal Society A 379 (2194). https://doi.org/10.1098/RSTA.2020.0097.

Setvák, M., Lindsey, D.T., Novák, P., Wang, P.K., Radová, M., Kerkmann, J., Grasso, L., Su, S.-H., Rabin, R.M., Šťástka, J., Charvát, Z., 2010. Satellite-observed cold-ring-shaped features atop deep convective clouds. Atmos. Res. 97 (1–2), 80–96. https://doi.org/10.1016/j.atmosres.2010.03.009.

Skamarock, W.C., Klemp, J.B., 1992. The stability of time-split numerical methods for the hydrostatic and the nonhydrostatic elastic equations. Mon. Weather Rev. 120 (9), 2109–2127. https://doi.org/10.1175/1520-0493(1992)120<2109:TSOTSN>2.0.CO;2.

Skripniková, K., Řezáčová, D., 2014. Radar-based hail detection. Atmosph. Res. 144, 175–185. https://doi.org/10.1016/J.ATMOSRES.2013.06.002.

Taszarek, M., Allen, J.T., Groenemeijer, P., Edwards, R., Brooks, H.E., Chmielewski, V., Enno, S.-E., 2020. Severe convective storms across Europe and the United States. Part I: climatology of lightning, large hail, severe wind, and tornadoes. J. Clim. 33 (23), 10239–10261. https://doi.org/10.1175/JCLI-D-20-0345.1.

Tiesi, A., Mazzà, S., Conte, D., Ricchi, A., Baldini, L., Montopoli, M., Picciotti, E., Vulpiani, G., Ferretti, R., Miglietta, M.M., 2022. Numerical simulation of a giant-hail-bearing mediterranean supercell in the Adriatic Sea. Atmosphere 13, 1219. https://doi.org/10.3390/atmos13081219.

Trapp, R.J., Davies-Jones, R., 1997. Tornadogenesis with and without a dynamic pipe effect. J. Atmos. Sci. 54 (1), 113–133. https://doi.org/10.1175/1520-0469(1997)054<0113:TWAWAD>2.0.CO;2.

Trapp, R.J., Stumpf, G.J., Manross, K.L., 2005. A reassessment of the percentage of tornadic mesocyclones. Weather Forecast. 20 (4), 680–687. https://doi.org/10.1175/WAF864.1.

Webb, J.D.C., Elsom, D.M., 2015. Severe Hailstorms in the United Kingdom and Ireland. In: Extreme Weather, pp. 155–194. https://doi.org/10.1002/9781118949986.CH9.